

1
2
3
4
5
6
7
8
9
10
11
12
13
14
15
16
17
18
19
20

This manuscript has been published in

Geochemical Perspectives Letters

with a slightly different title compared to previous versions posted here on Eartharxiv. This was done because of restrictions on the number of characters. In addition, the paper has been improved by the constructive reviews and we thank the reviewers for their help.

Please, support society-based, non-profit journals and cite the paper as:

Jelavić, S., Mitchell, A.C., Sand, K.K. (2020) Fate of organic compounds during transformation of ferrihydrite in iron formations. *Geochem. Persp. Let.* 15, 25–29.

<https://www.geochemicalperspectivesletters.org/article2030/>

21 **Fate of organic compounds during transformation of ferrihydrite in**
22 **iron formations**

23 S. Jelavić,^{1,2*} A.C. Mitchell³, K.K. Sand^{1,2,3}

24 ¹Nano-Science Center, Department of Chemistry, University of Copenhagen, Universitetsparken
25 5, Copenhagen, Denmark

26 ²Section for GeoGenetics, Globe Institute, University of Copenhagen, Øster Voldgade 5-7,
27 Copenhagen, Denmark

28 ³Aberystwyth University, Department of Geography & Earth Sciences, Aberystwyth, UK

29 *Corresponding author (email: stanislav.jelavic@sund.ku.dk)

30

31 **Abstract**

32 The absence of organic compounds from Precambrian iron formations (IF) challenges the
33 hypothesis of the biogenic origin of IF. Here we address the fate of adsorbed organic compounds
34 during transformation from ferrihydrite to hematite. We determined the binding energy between
35 hematite and common molecular terminations found in extracellular polymeric substances and
36 biofilms: carboxylic, hydroxyl and phosphate functional groups. We found that the bond between
37 hematite and hydroxyl groups is approximately 2 times stronger than the bond between hematite-
38 carboxyl and -phosphate groups. We transformed synthetic ferrihydrite to hematite at 90 °C in
39 presence of glycerol, which has a high density of hydroxyl groups and measured the amount of
40 mineral associated glycerol before and after the transformation. We show that the transformation
41 releases glycerol highlighting that organic compounds adsorbed at precursor ferrihydrite could be
42 desorbed during the process of IF sedimentation and diagenesis. Our results suggest that the
43 absence of organic compounds in IF should not be used as evidence against their biogenic origin.

44 **Introduction**

45 Traditionally, iron formations (IFs) have been considered as abiotically generated chemical
46 sediments but an increasing body of evidence suggests the active role of microbes in their
47 precipitation (Koehler *et al.*, 2010). The role of anoxygenic phototrophic bacteria in the formation
48 of IFs has been the object of speculation since the work of Garrels *et al.* (1973). An improved
49 understanding of microbially induced Fe(II) oxidation highlights that oxidising bacteria, such as
50 *Rhodobacter ferrooxidans*, could likely drive the formation of IFs (Kappler *et al.*, 2005). Further,
51 mass balance calculations have shown that Fe(II)-oxidising phototrophic bacteria have the capacity
52 to oxidise all Fe(II) from the Precambrian ocean, causing formation of iron (oxyhydr)oxide (FeOx)
53 (Hegler *et al.*, 2008). However, the low concentration of organic compounds in IFs and their
54 diagenetic or metamorphic derivatives, challenges the hypothesis of their biogenic origin (Klein,
55 2005).

56
57 Extracellular polymeric substances (EPS) promote FeOx nucleation (Sand *et al.*, 2020)
58 where microbially formed FeOx are often found in close association with the EPS (Chan *et al.*,
59 2004). When EPS is encrusted with FeOx, the polymers are shed and new EPS are formed. This
60 prevents the encrustation of the microbe itself (Phoenix *et al.*, 2000; Chan *et al.*, 2004). During IF
61 formation, FeOx-EPS composites would have settled through the water column and been deposited
62 on the sea floor. Some of the organic compounds were degraded by diagenetic and metamorphic
63 processes (Köhler *et al.*, 2013; Posth *et al.*, 2013; Halama *et al.*, 2016). In addition, there is
64 evidence that the depositional environment was most likely scarce in organic compounds (Dodd
65 *et al.*, 2019). Thus, the majority of the organic compounds was likely lost prior to deposition.

66
67 Hematite is a major component of IFs found today (Konhauser *et al.*, 2017) but, initially,
68 the FeOx in the FeOx-polymer complexes were most likely composed of ferrihydrite (Chan *et al.*,
69 2004). The transformation to hematite would have happened in aqueous solutions both before (Sun
70 *et al.*, 2015) and after deposition on the seabed. Depending on the solution conditions, ferrihydrite
71 to hematite transformation can involve intermediary phases such as lepidocrocite and goethite,
72 *e.g.*, through Fe(II) catalysed transformation (Hansel *et al.*, 2003), or it can be direct (Cudennec
73 and Lecerf, 2006). Transformation involving intermediary phases is a dissolution-precipitation
74 process (Schwertmann and Murad, 1983) implying that the interface between ferrihydrite and

75 organic compounds is eliminated. In this scenario, organic compounds would have been released
76 to solution where they could have been re-adsorbed but less strongly bound to newly formed
77 phases (Chen *et al.*, 2015), or released in the water column and subsequently degraded by various
78 biotic and abiotic processes (Kleber *et al.*, 2015). The direct transformation from ferrihydrite to
79 hematite is a solid-state transition where atoms move only locally to occupy new structural
80 positions (Cudennec and Lecerf, 2006), without the loss of an interface with adsorbed complexes.
81 Thus, the direct transformation of ferrihydrite to hematite is not necessarily accompanied by a
82 removal of organic compounds. However, the Gibbs free energy of binding (ΔG_{bu}) between
83 ferrihydrite and EPS is larger than between hematite and EPS (Sand *et al.*, 2020) implying that the
84 polymers were more likely to desorb from hematite than from ferrihydrite. In such a case, the
85 absence of organic compounds in IFs cannot be an argument against their biogenic origin.

86

87 To understand better the fate of adsorbed organic compounds during direct transformation
88 from ferrihydrite to hematite, we used dynamic force spectroscopy (DFS) to measure the energy
89 of binding between hematite and representative organic functional groups found in EPS.
90 Subsequently we identified the functional group least likely to desorb during transformation and
91 carried out transformation experiments where we used thermogravimetric analysis (TGA) to
92 measure the loss of organic compounds during transformation.

93

94 **Materials and Methods**

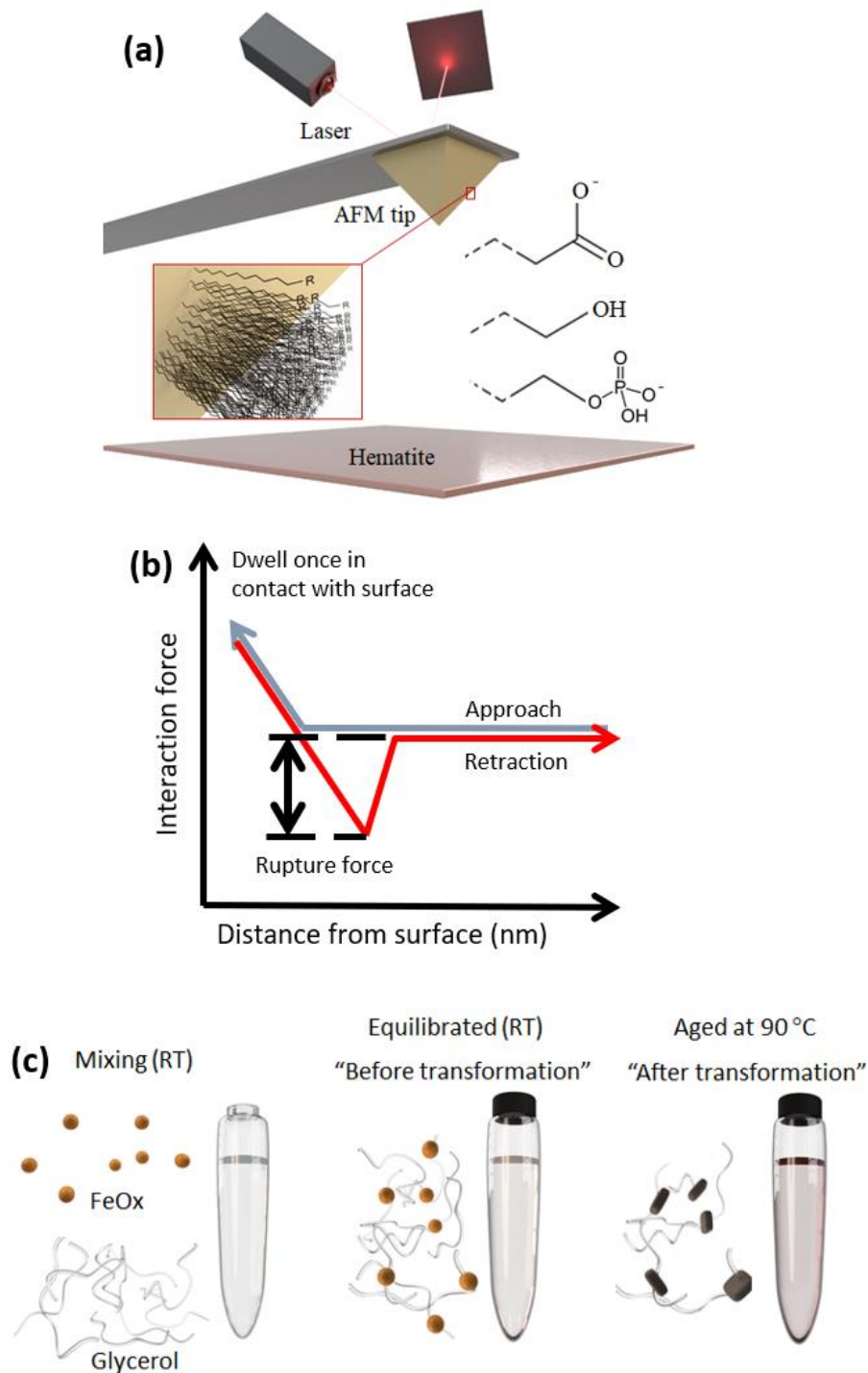
95 *DFS.* We used an Asylum MFP3D atomic force microscope (AFM) and functionalised
96 gold coated AFM tips (MSCT, Bruker) with carboxyl (COO^-), hydroxyl (OH), and phosphate
97 (HPO_4^-) headgroups pointing away from the AFM probe (Fig. 1a). Tips were functionalised
98 following the protocol described in Jelavić *et al.* (2017) (details in SI).

99

100 We used the {0001} face for DFS because it is one of the most common hematite surfaces
101 in the environment (Hartman, 1989) and because it is a predominant face on hematite produced by
102 transformation of ferrihydrite (Cornell and Schwertmann, 2004). The specular hematite
103 monocrystal {0001} face was cleaned prior to analysis following the protocol described in Jelavić
104 *et al.* (2017) (details in the SI). For DFS measurements, we collected >500 force curves *per*
105 experiment. The tip approaching velocity was set to 500 nm s^{-1} and the retraction velocity varied

106 between 10-10000 nms^{-1} . The trigger force was set to 100 pN and dwell time to 0.5 s. During the
107 measurement, the head groups bound to the hematite surface (Fig. 1a) and we measured the forces
108 applied to break the bond (*i.e.* the force curve, Fig. 1b). We fit the rupture forces *vs.* the loading
109 rate to a multibond model (Friddle *et al.*, 2012) enabling calculation of ΔG_{bu} (Eq. S-1 to Eq. S-4).
110 The measurements were done in 10 mM NaCl solution at pH = 5.6. We chose these conditions,
111 rather than conditions at which the transformation experiments were conducted, to maximise the
112 interaction forces between the tip and hematite surface (Lützenkirchen *et al.*, 2013; Newcomb *et*
113 *al.*, 2017).

114



115
116

117 **Figure 1** (a) Schematics of the DFS: self assembled monolayers with carboxyl, hydroxyl and
118 phosphate headgroups covalently bonded to AFM tip. (b) A scheme of a force curve. (c) In
119 transformation experiments, ferrihydrite and glycerol were mixed at room temperature and left to
120 equilibrate overnight. One sample was then taken for TGA (equilibrated sample) and the rest was
121 placed in the oven at 90 °C until the transformation was complete (aged sample).

122

123

124 **Transformation experiments.** Ferrihydrite was synthesised using the method of
125 Schwertmann and Cornell (2000). We used 0.5 M NaCl solution and pH = 7 as a proxy for
126 Precambrian seawater. We chose glycerol (CH₂OH-CHOH-CH₂OH) as a model for an OH-rich
127 molecule. Adsorption of polymers is a complex function of degree of branching, length and
128 hydrophobicity (van Oss, 1997). The aim here is not to account for such variations but to isolate
129 the effect of ΔG_{bu} , which is independent of those parameters, on the magnitude of desorption
130 during transformation. Coprecipitation of ferrihydrite-polymer aggregates results in a high organic
131 content compared to adsorbed polymers (Mikutta *et al.*, 2014) and can cause variations in grain
132 size and aggregation. To avoid any influence from such variations and to avoid low transformation
133 rates related to high surface coverage, we adsorbed glycerol to ferrihydrite in this study. We mixed
134 15 mg of ferrihydrite with 15 ml of 0.5 M NaCl and added glycerol to a final concentration of 0.5
135 % (Fig. 1c). In control samples, we omitted glycerol. Samples were shaken at 100 rpm overnight
136 to equilibrate. The next day, a batch of samples was rinsed with 20 ml of rinsing stock solution
137 (0.5 M NaCl adjusted to pH = 7 with 1 M NaOH) by ultra-centrifugation (equilibrated sample).
138 Another batch was placed in the oven heated to 90 °C. The samples from the oven were sampled
139 at specific time steps to follow the transformation pathway using X-ray diffraction (XRD). When
140 sampled, a batch was rinsed with 20 ml of 0.5 M NaCl and adjusted to pH = 7 (aged sample). All
141 samples were freeze dried after rinsing.

142

143 **XRD.** Samples for XRD were washed with ultra-deionised water. A volume of 1.5 ml of
144 suspension was pipetted on the zero background Si holders and left to dry at room temperature.
145 Such sample preparation results in large preferred orientation of anisotropic grains such as goethite
146 and lepidocrocite and allows us to detect minute quantities of crystalline material in a poorly
147 ordered matrix of ferrihydrite. We collected diffractograms in reflection mode on the Bruker D8
148 Advance instrument using Cu K α radiation ($\lambda = 1.5418 \text{ \AA}$) operated at 40 kV and 40 mA, and a
149 LynxEye detector. Diffractograms were collected from 10-90° 2 θ with step size of 0.02° and 1.7 s
150 counting time *per* step. The sample was spun at 20 rpm. We used 0.3° divergence and 3° antiscatter
151 slits, 2.5° Soller slits on incident and diffracted beams and a 0.02 mm thick Ni-filter. The opening
152 of detector window was 2.94°.

153

154 **TGA.** We used Netzsch TG 209 F1 Libra. Samples were heated at a rate of 10 °C min⁻¹
155 from 30 to 1000 °C under N₂ atmosphere. ~15 mg of sample were placed into the Pt crucible and
156 the weight loss was measured as a function of temperature.

157

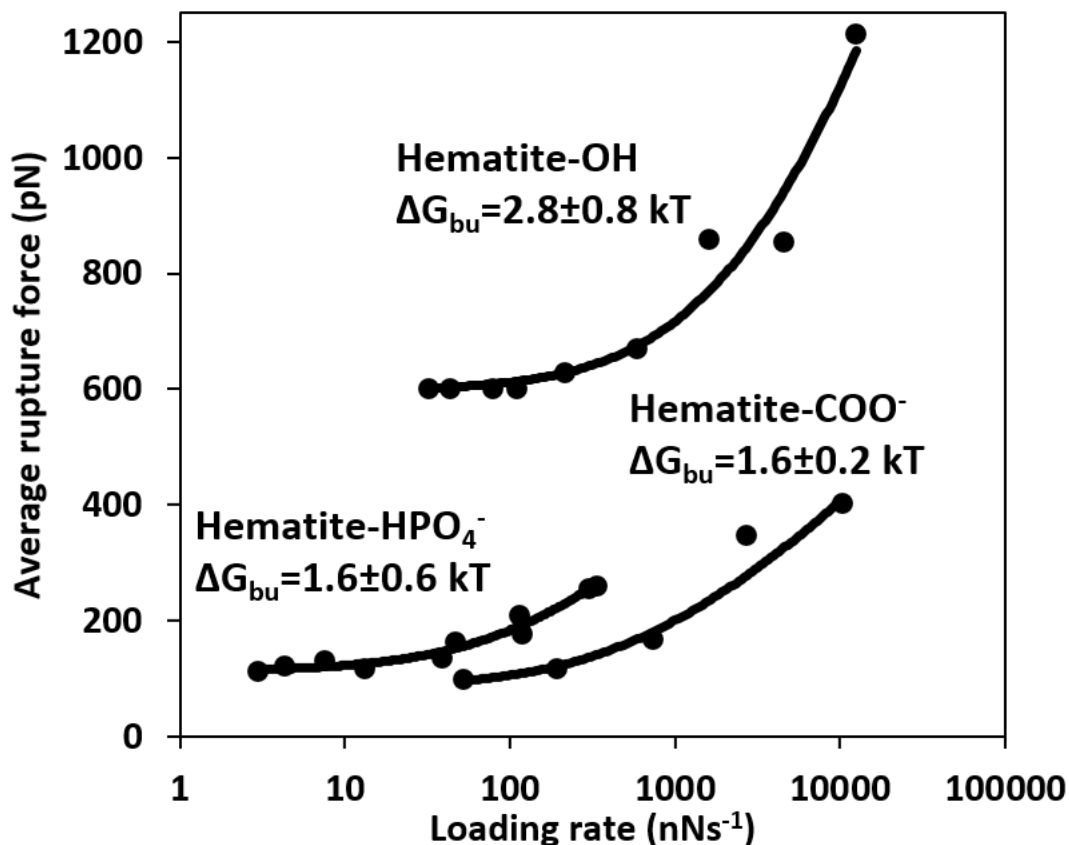
158 **TEM.** Images were taken with a Philips CM 20 TEM equipped with a thermionic LaB₆
159 filament. We used an accelerating voltage of 200 kV. Samples were prepared by placing a droplet
160 of sample suspension on a formvar coated TEM grid and left for 5-10 s. Subsequently, the grid
161 was washed in ultra-deionised water and water droplets were removed with the edge of a paper
162 towel.

163

164 **Results and Discussion**

165

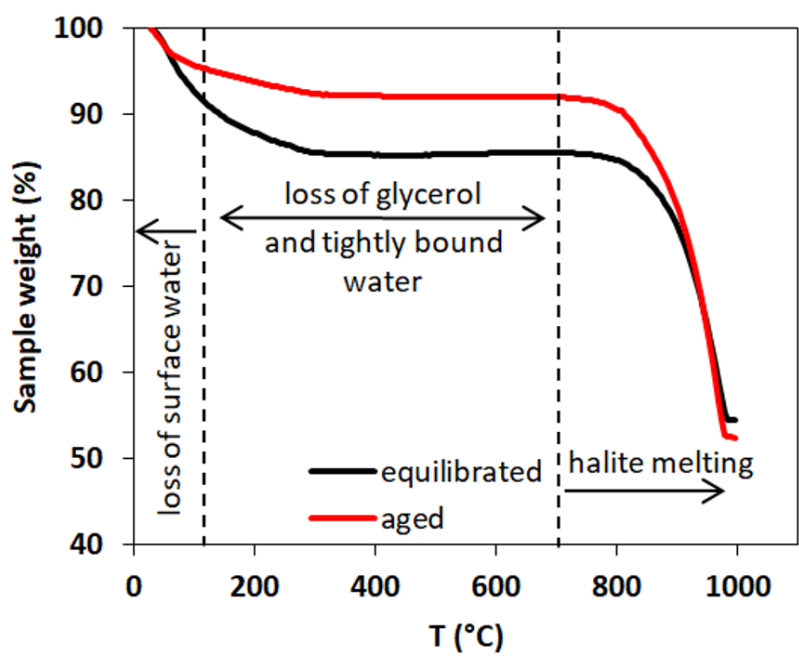
166 **Energy of binding.** The force spectra (Fig. 2) show that the rupture force between hematite
167 and the OH group is ~6 times higher than between COO⁻ and HPO₄⁻ groups (Fig. 2, Table S-1).
168 Recalculated to ΔG_{bu} (Eq. S-4), that is an increase in ~2 kT. These binding energies suggest that
169 the interaction is dominated by strong Van der Waals or weak electrostatic forces (Israelachvili,
170 2011). Considering that the {0001} hematite surface is completely hydroxylated in water (Trainor
171 *et al.*, 2004), our results follow the trend where OH-OH bonds are twice as strong as COO⁻-OH
172 bonds at circumneutral pH (Vezenov *et al.*, 1997) present in Precambrian ocean. Thus, irrespective
173 of the transformation pathway, biopolymers rich in acidic groups desorb more easily from hematite
174 than those rich in hydroxyl groups.



175
 176 **Figure 2** Multibond fit (Friddle *et al.*, 2012) to the dynamic force spectra between hematite surface
 177 and alkyl thiol self assembled monolayers with OH, HPO₄⁻ and COO⁻ head groups. The uncertainty
 178 represents the error propagated from the standard deviations of the fit. Loading rate is a nominal
 179 retraction velocity (nms⁻¹) multiplied with the spring constant of the cantilever (nNnm⁻¹).

180
 181 **Transformation pathway.** To investigate the fate of a ferrihydrite-associated OH-
 182 containing molecule during transformation to hematite, we transformed the ferrihydrite-glycerol
 183 complex, monitored the transformation pathway with XRD and determined the weight loss with
 184 TGA. The ferrihydrite-glycerol complex transformed directly to hematite without any intermediate
 185 phases detectable by XRD (Fig. S-3) suggesting a solid-state transformation pathway. As a control,
 186 we transformed ferrihydrite in absence of glycerol using the same solution conditions. Even though
 187 the hematite was the first phase to occur after 17 hr, goethite started forming after 43 hr (Fig. S-2)
 188 indicating that, in pure systems, some ferrihydrite dissolves and reprecipitates as goethite, as
 189 previously shown (Das *et al.*, 2011).

191 *The transformation is accompanied by glycerol release.* In general, the ferrihydrite-
 192 glycerol complex lost more weight than the pure ferrihydrite (Fig. 3, Table 1). Ferrihydrite is more
 193 hydrated than hematite so the loss of loosely adsorbed water (<125 °C) and tightly bound water
 194 (125-700 °C) is higher for ferrihydrite than hematite (Hiemstra and Van Riemsdijk, 2009).
 195 Comparing the weight loss of ferrihydrite-glycerol (5.4 %; Table 1) to pure ferrihydrite (4.7 %) in
 196 the 125-700 °C range, shows that the tightly bound water accounts only for 87 % of the weight
 197 loss in this region, indicating that the remaining 13 % is the loss of glycerol and associated
 198 interfacial water. This implies that hematite produced by aging ferrihydrite-glycerol contains less
 199 glycerol than the original ferrihydrite-glycerol (equilibrated), and that glycerol is released during
 200 transformation. Considering that the initial amount of adsorbed glycerol is ~5 mg/g of ferrihydrite
 201 (Fig. S-1), TGA indicates that all glycerol has been desorbed during the transformation.
 202



203
 204 **Figure 3** Comparison of TG curves of ferrihydrite-glycerol (equilibrium-black curve) and
 205 resulting hematite-glycerol (aged-red curve). The smaller mass loss in the region 125-700 °C
 206 (dashed vertical lines) for the aged sample compared to the equilibrium sample suggests bigger
 207 loss of tightly bound water and glycerol during the transformation.

208
 209
 210 **Table 1** Weight loss during the TGA analysis in <125 °C and 125-700 °C regions.

Sample		% weight loss	
		<125 °C	125-700 °C
Glycerol	equilibrated	8.9	5.4
	aged	4.8	3.2
Control	equilibrated	9.8	4.7
	aged	n.a.*	n.a.

211 * transformation yielded both goethite and hematite making comparison impossible

212

213 The reason for the loss of the glycerol during transformation can also be the smaller specific
214 surface area (SSA) of the produced hematite (Fig. S-4) and not only the lower affinity for glycerol
215 compared to ferrihydrite. From TEM images, we estimated the SSA of ferrihydrite to be 374-790
216 m^2g^{-1} and of hematite to be 10-46 m^2g^{-1} . Thus, the decrease in the SSA because of grain coarsening
217 during transformation is between 9-70 times which alone might explain the decrease in glycerol
218 content. However, the loss must be amplified by the lower ΔG_{bu} for hematite-OH than for
219 ferrihydrite-OH system. In addition, our thermodynamic results suggest that the loss of organic
220 compounds would have happened because of decreased ΔG_{bu} even if the subsequent grain
221 coarsening does not occur, *e.g.*, in case of hematite growth inhibition caused by organic
222 compounds. However, both scenarios are likely to have contributed to the loss of organic
223 compounds during the formation of IFs.

224

225 We have demonstrated that glycerol, a molecule with a high ΔG_{bu} to hematite, desorbs
226 during the transformation of ferrihydrite to hematite. We propose that a significant mass of organic
227 compounds from FeOx-EPS composites is desorbed early in the process of FeOx sedimentation
228 because of the transformation from ferrihydrite to hematite. This loss of organic compounds is
229 probably further enhanced by the grain coarsening of hematite during diagenetic and metamorphic
230 processes and concomitant reactions in the microenvironment that result in secondary
231 mineralisation, *e.g.*, Posth *et al.* (2013). Our experiments were designed to determine the loss of
232 strongly bound molecules from FeOx during the direct transformation, which is least likely to
233 result in desorption of adsorbed organic compounds. The less strongly bound organic compounds
234 or organic compounds adsorbed to ferrihydrite that transformed *via* dissolution-precipitation
235 pathway would likely have desorbed in higher proportion than that we report here. Thus, our results

236 highlight that the absence of organic compounds in IF should not be used as evidence against their
237 biogenic origin.

238

239 **Acknowledgements**

240 We thank Heloisa N. Bordallo for access to TGA instrument (Carlsbergfondets, grant no.
241 2013_01_0589). KKS and ACM are grateful for funding from the European Union's Horizon 2020
242 Research and Innovation Programme under Marie Skłodowska-Curie Grant Agreement No
243 663830 and the Welsh Government and Higher Education Funding Council for Wales through the
244 Sêr Cymru National Research Network for Low Carbon, Energy and Environment. KKS is grateful
245 for funding from the Danish Council for Independent Research Sapere Aude Programs (0602-
246 02654B).

247

248 **References**

- 249 Chan, C.S., Stasio, G.D., Welch, S.A., Girasole, M., Frazer, B.H., Nesterova, M.V., Fakra, S., Banfield, J.F.
250 (2004) Microbial Polysaccharides Template Assembly of Nanocrystal Fibers. *Science* 303, 1656–
251 1658.
- 252 Chen, C., Kukkadapu, R., Sparks, D.L. (2015) Influence of Coprecipitated Organic Matter on $\text{Fe}^{2+}_{(\text{aq})}$ -
253 Catalyzed Transformation of Ferrihydrite: Implications for Carbon Dynamics. *Environmental*
254 *Science & Technology* 49, 10927–10936.
- 255 Cornell, R.M., Schwertmann, U. (2004) Crystal Morphology and Size. In: *The Iron Oxides*. Wiley-VCH
256 Verlag Gmbh & Co., Weinheim, 59–94.
- 257 Cudennec, Y., Lecerf, A. (2006) The transformation of ferrihydrite into goethite or hematite, revisited.
258 *Journal of Solid State Chemistry* 179, 716–722.
- 259 Das, S., Hendry, M.J., Essilfie-Dughan, J. (2011) Transformation of Two-Line Ferrihydrite to Goethite and
260 Hematite as a Function of pH and Temperature. *Environmental Science & Technology* 45, 268–
261 275.
- 262 Dodd, M.S., Papineau, D., Pirajno, F., Wan, Y., Karhu, J.A. (2019) Minimal biomass deposition in banded
263 iron formations inferred from organic matter and clay relationships. *Nature Communications* 10,
264 1–13.

265 Friddle, R.W., Noy, A., Yoreo, J.J.D. (2012) Interpreting the widespread nonlinear force spectra of
266 intermolecular bonds. *Proceedings of the National Academy of Sciences* 109, 13573–13578.

267 Garrels, R.M., Perry, E.A., Mackenzie, F.T. (1973) Genesis of Precambrian Iron-Formations and the
268 Development of Atmospheric Oxygen. *Economic Geology* 68, 1173–1179.

269 Halama, M., Swanner, E.D., Konhauser, K.O., Kappler, A. (2016) Evaluation of siderite and magnetite
270 formation in BIFs by pressure–temperature experiments of Fe(III) minerals and microbial
271 biomass. *Earth and Planetary Science Letters* 450, 243–253.

272 Hansel, C.M., Benner, S.G., Neiss, J., Dohnalkova, A., Kukkadapu, R.K., Fendorf, S. (2003) Secondary
273 mineralization pathways induced by dissimilatory iron reduction of ferrihydrite under advective
274 flow. *Geochimica et Cosmochimica Acta* 67, 2977–2992.

275 Hartman, P. (1989) The effect of surface relaxation on crystal habit: Cases of corundum (α -Al₂O₃) and
276 Hematite (α -Fe₂O₃). *Journal of Crystal Growth* 96, 667–672.

277 Hegler, F., Posth, N.R., Jiang, J., Kappler, A. (2008) Physiology of phototrophic iron(II)-oxidizing bacteria:
278 implications for modern and ancient environments. *FEMS Microbiology Ecology* 66, 250–260.

279 Hiemstra, T., Van Riemsdijk, W.H. (2009) A surface structural model for ferrihydrite I: Sites related to
280 primary charge, molar mass, and mass density. *Geochimica et Cosmochimica Acta* 73, 4423–
281 4436.

282 Israelachvili, J.N. (2011) *Intermolecular and Surface Forces*. Third edition, Elsevier, Burlington.

283 Jelavić, S., Tobler, D.J., Hassenkam, T., Yoreo, J.J.D., Stipp, S.L.S., Sand, K.K. (2017) Prebiotic RNA
284 polymerisation: energetics of nucleotide adsorption and polymerisation on clay mineral
285 surfaces. *Chemical Communications* 53, 12700–12703.

286 Kappler, A., Pasquero, C., Konhauser, K.O., Newman, D.K. (2005) Deposition of banded iron formations
287 by anoxygenic phototrophic Fe(II)-oxidizing bacteria. *Geology* 33, 865–868.

288 Kleber, M., Eusterhues, K., Keiluweit, M., Mikutta, C., Mikutta, R., Nico, P.S. (2015) Chapter One -
289 Mineral–Organic Associations: Formation, Properties, and Relevance in Soil Environments. In:
290 Sparks, D.L. (Ed.) *Advances in Agronomy*. Academic Press, Cambridge, 1–140.

291 Klein, C. (2005) Some Precambrian banded iron-formations (BIFs) from around the world: Their age,
292 geologic setting, mineralogy, metamorphism, geochemistry, and origins. *American Mineralogist*
293 90, 1473–1499.

294 Koehler, I., Konhauser, K., Kappler, A. (2010) Role of Microorganisms in Banded Iron Formations. In:
295 Barton, L.L., Mandl, M., Loy, A (Eds.) *Geomicrobiology: Molecular and Environmental*
296 *Perspective*. Springer Netherlands, Dordrecht, 309–324.

297 Köhler, I., Konhauser, K.O., Papineau, D., Bekker, A., Kappler, A. (2013) Biological carbon precursor to
298 diagenetic siderite with spherical structures in iron formations. *Nature Communications* 4, 1–7.

299 Konhauser, K.O., Planavsky, N.J., Hardisty, D.S., Robbins, L.J., Warchola, T.J., Haugaard, R., Lalonde, S.V.,
300 Partin, C.A., Oonk, P.B.H., Tsikos, H., Lyons, T.W., Bekker, A., Johnson, C.M. (2017) Iron
301 formations: A global record of Neoproterozoic to Palaeoproterozoic environmental history. *Earth-*
302 *Science Reviews* 172, 140–177.

303 Lützenkirchen, J., Preočanin, T., Stipičić, F., Heberling, F., Rosenqvist, J., Kallay, N. (2013) Surface potential
304 at the hematite (001) crystal plane in aqueous environments and the effects of prolonged aging
305 in water. *Geochimica et Cosmochimica Acta* 120, 479–486.

306 Mikutta, R., Lorenz, D., Guggenberger, G., Haumaier, L., Freund, A. (2014) Properties and reactivity of Fe-
307 organic matter associations formed by coprecipitation versus adsorption: Clues from arsenate
308 batch adsorption. *Geochimica et Cosmochimica Acta* 144, 258–276.

309 Newcomb, C.J., Qafoku, N.P., Grate, J.W., Bailey, V.L., Yoreo, J.J.D. (2017) Developing a molecular picture
310 of soil organic matter–mineral interactions by quantifying organo–mineral binding. *Nature*
311 *Communications* 8, 396.

312 Oss, C.J. van (1997) Hydrophobicity and hydrophilicity of biosurfaces. *Current Opinion in Colloid &*
313 *Interface Science* 2, 503–512.

314 Phoenix, V.R., Adams, D.G., Konhauser, K.O. (2000) Cyanobacterial viability during hydrothermal
315 biomineralisation. *Chemical Geology* 169, 329–338.

316 Posth, N.R., Köhler, I., Swanner, E.D., Schröder, C., Wellmann, E., Binder, B., Konhauser, K.O., Neumann,
317 U., Berthold, C., Nowak, M., Kappler, A. (2013) Simulating Precambrian banded iron formation
318 diagenesis. *Chemical Geology*, Special Issue dedicated to H.D. Holland: Evolution of the
319 atmosphere and ocean through time 362, 66–73.

320 Sand, K.K., Jelavić, S., Dobberschütz, S., Ashby, P.D., Marshall, M.J., Dideriksen, K., Stipp, S.L.S., Kerisit,
321 S.N., Friddle, R.W., DeYoreo, J.J. (2020) Mechanistic insight into biopolymer induced iron oxide
322 mineralization through quantification of molecular bonding. *Nanoscale Advances* 2, 3323–3333.

323 Schwertmann, U., Cornell, R.M. (2000) Ferrihydrite. In: *Iron Oxides in the Laboratory*. John Wiley & Sons,
324 Ltd, Weinheim, 103–112.

325 Schwertmann, U., Murad, E. (1983) Effect of pH on the Formation of Goethite and Hematite from
326 Ferrihydrite. *Clays and Clay Minerals* 31, 277–284.

327 Sun, S., Konhauser, K.O., Kappler, A., Li, Y.-L. (2015) Primary hematite in Neoproterozoic to Paleoproterozoic
328 oceans. *GSA Bulletin* 127, 850–861.

- 329 Trainor, T.P., Chaka, A.M., Eng, P.J., Newville, M., Waychunas, G.A., Catalano, J.G., Brown, G.E. (2004)
330 Structure and reactivity of the hydrated hematite (0001) surface. *Surface Science* 573, 204–224.
- 331 Vezenov, D.V., Noy, A., Rozsnyai, L.F., Lieber, C.M. (1997) Force Titrations and Ionization State Sensitive
332 Imaging of Functional Groups in Aqueous Solutions by Chemical Force Microscopy. *Journal of*
333 *the American Chemical Society* 119, 2006–2015.
- 334